Glass dissolution rate measurement and calculation revisited

Maxime Fournier [a, *], Aurélien Ull [a], Elodie Nicoleau [a], Yaohiro Inagaki [b], Michaël Odorico [c], Pierre Frugier [a], Stéphane Gin [a]

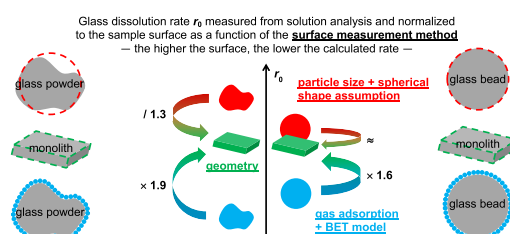[a] CEA, DEN, DTCD, SECM, F-30207, Bagnols sur Cèze, France
[b] Department of Applied Quantum Physics & Nuclear Engineering, Kyushu University, Fukuoka, 819-0395, Japan
[c] ICSM-UMR5257 CEA/CNRS/UM2/ENSCM, Site de Marcoule, BP17171, F-30207, Bagnols sur Cèze, France

HIGHLIGHTS

- Initial dissolution rates r_0 measured on glass particles or monoliths are compared.
- Repeatability of r_0 measurements and samples preparation procedure is quantified.
- Assimilating powders to spheres is the best way to estimate their reactive surface.
- r_0 (monolith) $= 0.8 \times r_0$ (powder, normalization to spherical geometric surface area).
- r_0 (monolith) $= 1.9 \times r_0$ (powder, normalization to BET surface area).

GRAPHICAL ABSTRACT

Glass dissolution rate r_0 measured from solution analysis and normalized to the sample surface as a function of the **surface measurement method** — the higher the surface, the lower the calculated rate —

ABSTRACT

Aqueous dissolution rate measurements of nuclear glasses are a key step in the long-term behavior study of such waste forms. These rates are routinely normalized to the glass surface area in contact with solution, and experiments are very often carried out using crushed materials. Various methods have been implemented to determine the surface area of such glass powders, leading to differing values, with the notion of the reactive surface area of crushed glass remaining vague. In this study, around forty initial dissolution rate measurements were conducted following static and flow rate (SPFT, MCFT) measurement protocols at 90 °C, pH 10. The international reference glass (ISG), in the forms of powders with different particle sizes and polished monoliths, and soda-lime glass beads were examined. Although crushed glass grains clearly cannot be assimilated with spheres, it is when using the samples geometric surface (S_{geo}) that the rates measured on powders are closest to those found for monoliths. Overestimation of the reactive surface when using the BET model (S_{BET}) may be due to small physical features at the atomic scale—contributing to BET surface area but not to AFM surface area. Such features are very small compared with the thickness of water ingress in glass (a few hundred nanometers) and should not be considered in rate calculations. With a S_{BET}/S_{geo} ratio of 2.5 ± 0.2 for ISG powders, it is shown here that rates measured on powders and normalized to S_{geo} should be divided by 1.3 and rates normalized to S_{BET} should be multiplied by 1.9 in order to be compared with rates measured on a monolith. The use of glass beads indicates that the geometric surface gives a good estimation of glass reactive surface if sample geometry can be precisely described. Although data clearly shows the repeatability of measurements, results must be given with a high uncertainty of approximately ±25%.

© 2016 Elsevier B.V. All rights reserved.

* Corresponding author.
  E-mail address: maxime.fournier@cea.fr (M. Fournier).

1. Introduction

The vitrification of high level waste from spent fuel reprocessing and the choice of the geological disposal force many countries (France, Japan, United Kingdom, etc.) to study the long term behavior of borosilicate glass waste form [1,2]. Under disposal conditions, the main cause of glass degradation is aqueous dissolution. To assess the environmental impact and ensure the safety of the geological disposal, glass alteration studies are essential. Radionuclide release depends primarily on the glass dissolution rate, which is directly related to the glass surface in contact with water.

Many tests have been standardized to identify waste glass dissolution parameters and mechanisms [3]. These tests—under static or flow rate conditions—simulate a wide variety of experimental conditions and use glass monoliths or powders obtained by crushing. The design of these tests routinely involves the glass surface in contact with the leachant volume as a dimensioning parameter. In addition to experiments, the study of glass long-term behavior uses modeling to access the very long time scales [4,5]. The quality of predictions of geochemical models is particularly dependent on "reactive" surface data to efficiently describe interfacial mechanisms such as dissolution. The "reactive" surface is defined here as the glass-water interfacial area. There is currently no consensus on how to determine this surface area; indeed, such difficulties can be partially explained by the fact that geometric and specific surface areas are rarely equal for physical—e.g. porosity—or chemical—e.g. surface sites reactivity—reasons.

For decades, experimenters determined glass waste form dissolution rates by using powders (e.g. Refs. [6–16]). There are two common ways to estimate glass reactive surface: physisorption of gaseous molecules or geometric considerations. Calculations based on gas molecule physisorption require an estimate of the gas cross sectional area and of the amount of gas necessary to form a monolayer on the powdered sample. The specific surface area is then evaluated by the application of Brunauer-Emmett-Teller (BET) equations [17] to nitrogen or krypton adsorption data.

By assuming particles have a certain geometry (glass grains are usually treated as spheres, or more rarely as cubes [18]), the geometric surface area can be calculated as a function of particle size. Assuming a spherical geometry for smooth non-porous glass grains with normally distributed sizes, the geometric surface area of a particle is calculated using Eq. (1) [19] where S_{geo} is the glass surface ($m^2 \, kg^{-1}$), ρ the glass density ($kg \, m^{-3}$) and R the average radius of the particles (m). Note that the estimation of the average radius R requires an—often implicit—assumption on the distribution of the radius of the grains, their surface area or volume. The arithmetic mean $(R_{min} + R_{max})/2$ is the most commonly used; the quadratic mean or other estimators may also be encountered [20].

$$S_{geo} = \frac{3}{\rho \cdot R} \qquad (1)$$

Surface measured by the BET method systematically gives higher values than geometric measurements, that lead to a debate in the community about the surface that should be used as the glass "reactive" surface. The S_{BET}/S_{geo} ratio is interpreted to be representative of the irregular shapes and surface roughness of glass particles [21–26]. In the case of glass powders, the extent of S_{BET} can also indicate the presence of finer-grained particles produced by glass crushing and adherent to glass grains of the required size fraction [21,22]. These fine particles develop a large specific surface. Pierce et al. gave S_{BET}/S_{geo} values between 1.6 and 4.5 [21,22,27].

Glass dissolution rate—always announced relatively to the glass surface—is then calculated by mass balance from Eq. (2) [28] where r is the dissolution rate ($g \, m^{-2} \, d^{-1}$), m_i the amount of tracer i leached during the time Δt, m_{i0} the amount of tracer i in the pristine glass and S the so-called glass reactive surface. An iterative version of Eqs. (1) and (2) is used to take into account the evolution of the surface due to the loss of material from the glass over time. These calculations are of primary importance because the maximum release limit of radionuclides is conditioned by the release of glass constituents that are known to be alteration tracers (e.g. for borosilicate waste glass, boron or lithium if present at >1 wt.% [29]). Tracers are not retained in secondary amorphous or crystalline phases formed during glass alteration.

$$r = \frac{m_i}{S \cdot \Delta t \cdot m_{i0}} \qquad (2)$$

One wonders what glass surface determination method gives a "true" value for glass dissolution rate, i.e. what is the glass reactive surface area with respect to its dissolution. It is generally considered that the rate calculated from the geometric surface area of monoliths—with at least the two larger sides that are optical-grade polished—is a practical reference. Experiments conducted with SON68 glass (inactive surrogate of French R7T7 nuclear glass) as powders and monoliths in a single-pass flow-through system with the same flow-to-surface area ratio [30] show that the dissolution rate values obtained for powders, with normalization to their geometric surface area, coincide with those obtained for monoliths. In comparison, the rates normalized to BET surface area are slower and generally outside the 2σ experimental uncertainty. The same conclusions were drawn by Inagaki et al. [31] (on the International Simple Glass) and by Pierce et al. [21,22] (on various American low-activity waste glasses) in comparisons of their own experimental data with the literature. Although the experimental evidence cannot be doubted, these results are surprising because glass grains are obviously not spherical and their surface irregularities are not taken into account when calculating the geometric surface area from Eq. (1). Furthermore, it is noted that cases also exist—though they are more rare—where rate calculations normalized to the BET surface area are comparable to rates measured on monoliths [32].

Such questions also exist to determine the reactive surface of natural glasses [33] or crystals [34]. The use of the geometric surface is advised by Wolf-Boenisch et al. [33] (on natural glasses) and Gautier et al. [35] (on quartz grains) because it is considered to be more representative of the reactive surface of such materials. However, Jeschke and Dreybrodt [36] indicate that the dissolution rate of a mineral is related to its morphology: the geometric surface may be used only when the rate constant of the reaction (depending on the reactive surface) is small compared to the mass transport constant D/ε, where D is the diffusion coefficient in the thickness ε of the alteration layer.

In this paper, initial dissolution rates measured on glass particles and monoliths were compared. The initial dissolution rate was chosen because it is the most favorable glass alteration regime for precise rate measurements. Rates determined on particle samples were normalized to geometric or specific surface areas measured by gas adsorption. The aim of the authors is to give quantitative elements for the comparison of results achieved by the international teams working on the subject, according to their experimental protocols. This paper also considers the uncertainties related to alteration rates measurements. Finally this study gives the opportunity to answer questions related to the relevance of crushing and washing protocols and to the repeatability of rate measurements.

2. Material and methods

2.1. Glass sample preparation

The majority of experiments presented in this paper were performed on International Simple Glass (ISG), an alumino-borosilicate glass composed of six oxides (Table 1) chosen to be a reference glass for international studies on waste glass dissolution [2] and prepared by Mo-Sci Corporation (Rolla, MO, USA) as described elsewhere [37]. Powders were prepared by successive crushing steps with a vario-planetary mill (Fritsch Pulverisette 5) with hardmetal tungsten carbide grinding balls and bowls. Rotation speed was close to 100 rpm for periods ranging from a few seconds to a few minutes, depending on the particle sizes that had to be obtained. Between each crushing step, the glass was sieved (Retsch AS 200 analytical sieve shaker) for several minutes to obtain the desired particles sizes, then oversized particles were crushed again. The different particles size fractions were washed by an iterative decantation process in acetone and absolute ethanol to remove fine particles, according to Stokes' law (see Eq. (3), where r_s is the sedimentation rate, R_{min} the diameter of the smallest particle, g the gravitational acceleration, ρ_p and ρ_s the mass densities of the powder and the solvent, and η_s the dynamic viscosity of the solvent), until the supernatant was clear.

$$r_s = \frac{2 \cdot R_{min}^2 \cdot g \cdot \left(\rho_p - \rho_s \right)}{9 \cdot \eta_s} \tag{3}$$

The 63–125 μm size fraction was prepared in five completely independent batches (separate crushing, sieving and washing) to test the effects of sample preparation and measurement repeatability. Note that repeatability is defined as the "precision under conditions where independent test results are obtained with the same method on identical test items in the same laboratory by the same operator using the same equipment within short intervals of time" [38,39]. The 63–125 μm sample size fraction was used for most of the experiments. The effects of particle size were also tested using 20–40 μm, 40–63 μm and 125–250 μm size fractions.

To test the effect of particle shape, some experiments were also performed on SiLibeads® (Sigmung Lindner) Type S glass beads (Table 1) produced from soda lime glass through a thermal rounding process. Glass beads have a homogenous smooth surface, and quite high roundness. The size ranges selected for this study were 90–150 μm, 150–250 μm, 250–500 μm, 500–750 μm and 750–1000 μm.

Dissolution rates measured on powders or beads were compared to those measured on glass monoliths. For both glasses (ISG and Type S), glass coupons of approximately 2.5 cm × 2.5 cm × 2 mm were cut from glass bars using a diamond saw (except for the microchannel flow-through test, for which ISG monoliths of 3 cm × 1 cm × 4 mm were used to fit the apparatus). Angles between edges and adjacent faces were 90°. The six faces were abraded to a reflective sheen using a Struers Abramin polishing device and successively 220, 500, 800, 1200 and 2400-grit SiC abrasive papers. Final polishing was done with 6 μm, 3 μm and 1 μm cloths and diamond suspensions. For each step, the

sample holder rotated at 150 rpm and the plate at 150 rpm for 90 s with the press-on force increasing from 0 to 20 N and 300 rpm for 60 s with the press-on force increasing from 20 to 30 N.

Scanning electron microscopy (SEM, Zeiss Supra™ 55) observations were carried out on powder and bead samples to better describe their morphology and surface state.

2.2. Annealing

Some experiments were conducted on glass samples annealed after their preparation. 63–125 μm ISG glass powder and ISG glass monoliths were thermally annealed at $0.9 \times T_g$ for 2 h [40] ($T_g = 843$ K [41] is the transition temperature of the glass). After this step, the glass was cooled at 1 °C min^{-1} to room temperature. Powder samples were placed in a Pt-Rh crucible, and monoliths were positioned to minimize contacts between the glass and its support inside the furnace.

2.3. Glass powder and bead size distribution

Laser diffraction (Malvern Mastersizer 3000) was used to calculate particle size distribution by measuring the angular variation in the scattered light intensity produced by a laser beam passing through a dispersed particulate sample. The angular scattering intensity data was analyzed to calculate the size of the particles responsible for creating the scattering pattern, using the Mie theory and assuming a volume equivalent sphere model. Refractive indices were taken equal to 1.54 for ISG glass, 1.52 for Type S glass beads [42] and 1.33 for the dispersant (water). The results were divided into 100 size fractions logarithmically distributed between 10^{-2} and $3 \cdot 10^3$ μm.

2.4. Glass surface measurements

2.4.1. Specific surface area of powders and beads

The specific surface area of ISG glass powders and Type S glass beads were measured by krypton physical adsorption on the sample surface (Micromeritics ASAP 2020). All samples were outgassed at 200 °C under vacuum of 0.13 Pa minimum during 4 h.

Such types of measurements require the estimation of the amount of adsorbate gas needed to form a monolayer on the solid surface. This monolayer capacity could be estimated by several models, among which the BET model [17] is the best-known, and given in Eq. (4) where V_g is the volume of gas adsorbed, V_m the volume of gas adsorbed to produce a monolayer on the sample surface, p the partial vapor pressure of adsorbate gas at equilibrium with the surface at liquid nitrogen temperature (≈ 77 K), p_0 the saturation pressure of adsorbate gas and c the BET constant related to the adsorbate gas adsorption enthalpy.

$$\frac{1}{V_g \cdot \left(\frac{p_0}{p} - 1 \right)} = \frac{c-1}{V_m \cdot c} \cdot \frac{p}{p_0} + \frac{1}{V_m \cdot c} \tag{4}$$

The specific surface area S_{BET} is then calculated from V_m by Eq. (5), where N_A is the Avogadro constant, a the area occupied by one

Table 1
International Simple Glass (ISG) and Type S SiLibeads® glass beads compositions expressed in oxide weight percent.

ISG [62]	SiO$_2$	B$_2$O$_3$	Na$_2$O	Al$_2$O$_3$	CaO	ZrO$_2$
Oxide wt%	56.2 ± 1.5	17.3 ± 0.9	12.2 ± 0.7	6.1 ± 0.8	5.0 ± 0.6	3.3 ± 0.5
Type S SiLibeads® [42]	SiO$_2$	Na$_2$O	CaO	MgO	Al$_2$O$_3$	
Oxide wt.%	72.50 ± 0.90	13.00 ± 0.80	9.06 ± 0.28	4.22 ± 0.10	0.58 ± 0.18	

molecule of adsorbate gas (20 $Å^2$ for Kr), m the mass of powder and 22,400 mL the volume occupied by 1 mol of adsorbate gas at STP.

$$S_{BET} = \frac{V_m \cdot N_A \cdot a}{m \cdot 22400} \qquad (5)$$

It should be noted here that such measurements cannot be performed on glass monoliths, because their surface area is far too low.

2.4.2. Geometric surface areas

The geometric surface areas of powders and beads were calculated using Eq. (1), assuming a spherical geometry for powders with a mean radius being the mid-value of the interval between the sieve openings (e.g. 94 μm for 63–125 μm glass grains). This is the easiest and most employed method to estimate the value of the mean radius R.

Using the particle size distribution (section 2.2), it was possible to recalculate the geometric surface area $S_{geo-psd}$ developed by particle samples more accurately, by weighting Eq. (1) with the statistical distribution $\%n_j$ of each of the j size classes centered on the particle radius R_j (Eq. (6)). $\%n_j$ was deduced from the volume equivalent sphere model data $\%V_j$ given by laser diffraction, using Eq. (7) applied to the i size classes considered.

$$S_{geo-psd} = \sum_j \%n_j \cdot \frac{3}{\rho \cdot R_j} \qquad (6)$$

$$\%n_j = 100 \cdot \frac{\frac{3 \cdot \%V_j}{4 \cdot \pi \cdot R_j^3}}{\sum_i \frac{3 \cdot \%V_i}{4 \cdot \pi \cdot R_i^3}} \qquad (7)$$

The geometric surface areas of monoliths were determined by measuring their dimensions using a digital caliper with a precision of ±0.02 mm.

2.5. Atomic force microscopy

Atomic force microscopy (AFM) experiments were performed with a commercial AFM, Multimode 8 and Nanoscope V controller (Veeco, Santa Barbara, CA). Glass particles were imaged in Tapping mode with RTESP antimony (n) doped silicium tips ($K = 40$ N/nm, $f_0 = 300$ kHz from Bruker). Free amplitude was set around 1 V. Glass monoliths were imaged in Peak Force mode with a SNL silicon tip on Nitride lever ($K = 0.35$ N/nm, from Bruker). Force was set around 100 pN.

Measured topography data were processed by NanoScope Analysis software v1.40 (Bruker Corporation) to calculate R_a (Eq. (8)) the arithmetic average of the absolute values of the surface height deviations measured from the mean plane and R_{ms} (Eq. (9)) the root mean square average of height deviations taken from the mean image data plane. The surface area difference ΔS representing the difference between the analyzed region's three dimensional surface area and its two-dimensional, footprint area was also calculated.

$$R_a = \frac{1}{N} \cdot \sum_{i=1}^{N} |y_i| \qquad (8)$$

$$R_{ms} = \sqrt{\frac{1}{N} \cdot \sum_{i=1}^{N} y_i^2} \qquad (9)$$

2.6. Leaching tests

2.6.1. Leaching solution

For all experimental procedures described below, dedicated to initial rate measurements, the leaching solution consisted of a KOH solution giving a pH 10 ± 0.1 measured at 90 °C. These conditions were chosen because the resulting glass dissolution rates could be expected to be of a few g m^{-2} d^{-1}, high enough for accurate solution analysis.

2.6.2. Static leaching experiments

The initial dissolution rate, r_0, was primarily determined by static leaching tests (ST) at 90 ± 2 °C. The test vessel was a Perfluoroalkoxy (PFA) reactor in which the solution was continuously homogenized by a magnetic stirring rod. Solution samples were taken at regular intervals and analyzed by spectrophotometry (see section 2.7). pH was measured at the beginning and end of all tests: the deviation during experiments was always less than 0.1 pH unit. In addition, adapted test durations permit to achieve altered glass thicknesses of several hundred nanometers to overcome difficulties linked to compositional differences of the sample extreme surface due to polishing [41].

Throughout the experiment, the solution was always sufficiently diluted ([Si] < 3 mg L^{-1} = 0.1 mmol L^{-1}). The rate drop following the initial dissolution rate regime which was to be avoided in these tests can be recognized by a difference in the apparent saturation measured. For ISG glass at 90 °C pH 9, the rate drop leads to a plateau for silica activity when [H_4SiO_4] ≈ 2.5 mmol L^{-1} [11] (this value will be higher at 90 °C pH 10), whereas the maximum silica concentration in these experiments was more than 25 times lower than this activity. The glass surface area to solution volume ratio (S/V) calculations for the experiment design were based on S_{BET} for powders and beads and S_{geo} for monoliths. The same ratio was used for experiments on particle samples and monoliths (around 7 m^{-1}). Note that this ratio has no influence on r_0 as long as the solution remains sufficiently diluted.

2.6.3. Single-pass flow-through test

The initial dissolution rate was also measured in a single-pass flow-through test (SPFT) at 90 ± 2 °C. The principle is to pass a leaching solution at a high flow rate over glass powder, to avoid any feedback effect on the rate from glass constituent elements released into solution. The test reactor was a Polytetrafluoroethylene (PTFE) tube column, 4 mm in diameter and 5 cm long. The leaching solution temperature was monitored continuously at the reactor inlet. Approximately 100 mg of glass powder were inserted in the column for each rate measurement. The solution flow rate to glass surface area (Q/S) was about 1 m d^{-1} (≈ 10 L d^{-1}).

2.6.4. Microchannel flow-through test

The microchannel flow-through test (MCFT) [31,43–46] apparatus consists of an injection syringe pump, a PFA microchannel reactor unit (placed in an oven at 90 °C) and an automatic sampler, all connected with each other by PTFE (Teflon®) tubing. In the microchannel reactor unit, a face of the glass monolith specimen is in contact with a microchannel (20 mm length, 2 mm width, 0.16 mm depth) where the solution flows at a constant rate (20 μL min^{-1}). The apparent S/V ratio was estimated to be 6400 m^{-1}. The Reynolds number was calculated to be less than 0.5, which indicated that the solution flow regime was a completely laminar flow.

2.7. Solution analyses

The dissolved silica concentrations used for initial rate

calculations were determined photometrically (Merck Spectroquant® Silicate Test, Cary® 50 Scan UV−Vis spectrophotometer) with a method analogous to ASTM D859-10 [47]. Basically, in a sulfuric solution silicate ions react with molybdate ions to form a yellow heteropolyacid ($H_4SiMo_{12}O_{40}$). This was reduced by 1-amino-2-naphthol-4-sulfonic acid to silicomolybdenum blue, which was measured photometrically at 820 nm. The measuring range of the technique is 0.1−3 mg L^{-1} of Si. Spectrophotometer calibration was performed before each measurement and was accepted only if the correlation coefficient of the calibration curve was greater than 0.999. From the silicon concentrations, Eq. (2) was used to calculate the dissolution rate. Linear regression on Si release was performed on a minimum of seven points (including the graph origin), and the correlation coefficient was always greater than 0.99.

After dilution with ultra-pure grade 65 wt% HNO_3, concentrations of Si, B, Na, Al, Ca, Zr (for ISG glass) and Si, Na, Ca, Mg, Al (for Type S glass beads glass) were determined by ICP-OES (Thermo Scientific iCAP™ 6000 Series) for some samples, to check (i) the repeatability of the silicon concentration determination, (ii) the congruence of dissolution and (iii) the linearity of the main glass component releases. The quantification limits were 2, 10, 10, 20, 20, 20 and 20 μg L^{-1} for Zr, Al, Si, B, Ca, Li and Na respectively. The background concentrations in the starting solution were systematically below the detection limits, except for K and Na because of traces of Na present in the KOH solution. Zr was systematically below the detection limit. Note that for MCFT tests, an Agilent Technologies ICP-MS 7500c was employed.

3. Results

3.1. Glass sample surface area measurements

3.1.1. Particle size distribution and geometric surface area calculations

For ISG glass powders and Type S glass beads used for leaching experiments, S_{geo} and $S_{geo-psd}$ were calculated, taking into account particle size distributions evaluated from laser diffraction, using Eqs. (1) and (6) respectively. As laser diffraction results are reported on a volume basis, Eq. (7) was used to convert data into number distributions. The results are reported in Table 2.

The ISG glass particles size distribution for five powder batches of the same size fraction prepared independently using the same protocol is comparable (Fig. 1), which demonstrates the good repeatability of the powder preparation procedure (crushing, sieving and washing, see section 2.1). Fig. 2a shows the particle size distribution of an ISG glass powder batch sieved between 63 and 125 μm: considering the %n curve, overly large and small grains can be observed compared to those expected from the sieve mesh sizes. The SEM image (Fig. 2b) is quite in agreement with the size expected from the sieves. These conclusions can be extended to all ISG size fractions (Fig. 3). Above-limit particle sizes therefore do not seem to be over-estimated as a result of spherical grain assumption made when calculating particle size with laser diffraction.

To assess the impact of the particles geometry on the surface area they develop, it was of particular interest to consider glass particles with a spherical shape. Particle size distributions for Type S glass beads are presented in Fig. 4a: (i) beads with a diameter < 250 μm (Fig. 4b−c) have a wide size distribution and are polluted with a small amount of non-spherical waste; (ii) for beads with a diameter > 250 μm (Fig. 4d−f), the fraction of beads outside the range advertised by the manufacturer is low; the presence of overly-large particles might be explained by the protuberances visible on the surface of some beads or by ovoid particles that distort their radius measurement.

Nevertheless, the particle size distribution curves for the two glasses are close to a Gaussian shape. Therefore, S_{geo} and $S_{geo-psd}$ surfaces are close (Table 2), with a maximum deviation of 10%.

3.1.2. Specific surface area measurements

Results obtained by physical adsorption of gas and application of the BET method are presented in Table 2.

The standard deviation of measurements on the five ISG 63−125 μm independently prepared powder batches ($\sigma = 21$ cm² g⁻¹) is well below the 10% accuracy usually given for this type of measurement [48]. The five powder batches can be considered identical, with a mean value at 630 cm² g⁻¹. Data from specific surface area measurements were compared to the geometric surface areas S_{geo} and $S_{geo-psd}$. For ISG glass, the $S_{BET}/S_{geo-psd}$ ratio of 2.5 ± 0.2 illustrates the difference between an actual glass grain and a smooth sphere in terms of morphology and surface roughness. As the dissolution rates are normalized to the glass surface, this ratio is equal to the factor between rates normalized to the BET specific or to the geometric surface areas.

For Type S glass beads, the proximity of the bead shape to that of a sphere (sphericity of these particles was evaluated between 0.92 and 0.97 [65]) reduces the $S_{BET}/S_{geo-psd}$ ratio to 1.7 ± 0.4. The surface measurements are consistent with those carried out by Zellnitz et al. [65] on the same materials (whose surface was however washed with a different procedure). Nevertheless the S_{BET}/S_{geo} ratio remains greater than 1 presumably because glass beads present surface features accessible to gas molecules. This hypothesis is consistent with the results: the $S_{BET}/S_{geo-psd}$ ratio is indeed higher for larger particles, for which the contribution of external surface to the total surface area decreases in favor of the surface contribution due to roughness.

3.1.3. Characterization of glass samples roughness by AFM
3.1.3.1. Type S glass beads.
AFM analyses were conducted on three different particle sizes (150−250 μm, 500−750 μm and 750−1000 μm) and at least on three beads for each particle size. Tests have shown that a stabilized roughness measurement is provided by a pixel size ≤5 nm. 10 μm × 10 μm images were thus produced with a resolution of 5 nm per pixel (e.g. Fig. 5a). In Fig. 5b, the vertical height scale is 20 times relative to the horizontal scale, the maximum vertical relief is ≈215 nm Fig. 5c shows the homogeneity of the surface developed by the beads within each particle size but heterogeneous results from one particle size to another. The roughness of beads surface causes a surface area increase ΔS ranging from ≈2% (150−250 μm) to ≈10% (500−750 μm).

3.1.3.2. ISG glass powders.
AFM analyzes were conducted on the two larger particle sizes (63−125 μm and 125−250 μm). The only areas on which a measurement is possible are those near the upper surface of the particles and oriented in parallel to the scanning plane. On these areas, ΔS varies from 2% ($R_{ms} \approx 15$ nm) to 30% ($R_{ms} \approx 450$ nm) for analyzed regions. Such discrepancies show that the surface of the grains is too heterogeneous (e.g. many steps due to conchoidal fractures, Fig. 6) to allow an extrapolation of these results to the entire surface of the particles. AFM cannot be used to determine the roughness of crushed glass grains, only a lower bound of this parameter can be inferred.

3.1.3.3. ISG glass monolith.
5 × 5 μm and 10 × 10 μm AFM images of the polished ISG surface show smooth and flat surface that present randomly distributed scratches (Fig. 7). Average roughness values for polished monolith are $R_a = 1.18$ nm and $R_{ms} = 1.60$ nm; these values are consistent with those obtained on other polished glass samples: some examples are summarized in Table 3. The differences can be explained by the different polishing protocols used

Table 2
Comparison of specific surface areas determined by gas adsorption (BET model, S_{BET}), geometric surface areas assuming a spherical shape for glass grains (Eq. (1), S_{geo}) and geometric surface areas taking into account particle size distributions within the sample (Eqs. (6) and (7), $S_{geo-psd}$). Five batches of 63−125 μm ISG glass size fraction (B1 to B5) were prepared independently. $|\Delta_{geo/geo-psd}|$ represents the absolute value of the difference between $S_{geo-psd}$ and S_{geo}.

Glass	Size fraction (μm)	S_{BET} (cm² g⁻¹)	S_{geo} (cm² g⁻¹)	$S_{geo-psd}$ (cm² g⁻¹)	$|\Delta_{geo/geo-psd}|$ (%)	$S_{BET}/S_{geo-psd}$
ISG	20−40	2065	800	754	5.8	2.7
ISG	40−63	1120	466	440	5.6	2.5
ISG	63−125 B1	635	255	256	0.4	2.5
ISG	63−125 B2	645	255	239	6.3	2.7
ISG	63−125 B3	655	255	253	0.8	2.6
ISG	63−125 B4	630	255	248	2.7	2.5
ISG	63−125 B5	600	255	259	1.6	2.3
ISG	125−250	345	128	133	3.9	2.6
Type S	90−150	270	200	200	0.0	1.4
Type S	150−250	155	120	109	9.2	1.4
Type S	250−500	125	64	59	7.8	2.1
Type S	500−750	75	38	35	7.9	2.1
Type S	750−1000	51	27	25	7.4	2.0
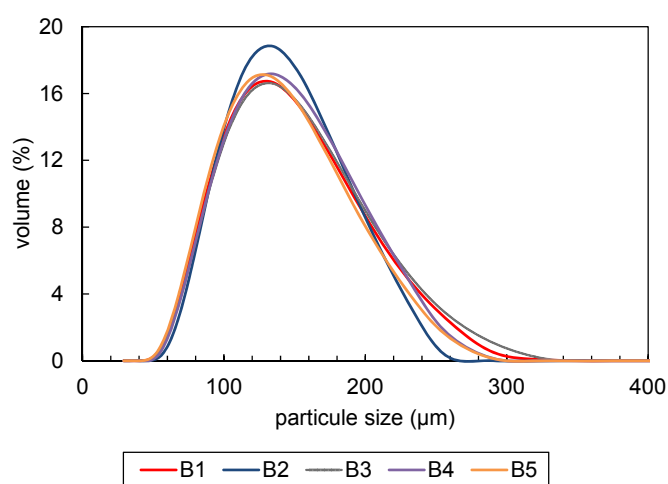
Fig. 1. Statistical particle size distributions (volume distribution %V) for the five ISG glass independently prepared powder batches (63−125 μm).

and the different glass compositions. For ISG sample, ΔS representing the difference between the three dimensional surface area and its footprint area is less than 1%.

### 3.2. Post-treatment effects on glass surface area

The impacts of two types of post-treatments on the BET specific surface area and particle size distribution were tested (washing and annealing).

3.2.1. Washing with water

Washing glass powder with water (a technique sometimes used to remove fine particles after crushing [21,22]) may cause a small glass dissolution, and thus create a tiny but potentially rough or porous alteration layer which could contribute to the surface area measured by gas physisorption. This hypothesis was tested by placing ISG glass powder and Type S glass beads in contact with water for 15 min at room temperature (realistic conditions for a glass powder washing). After washing, the specific surface area (Table 4) remained in the interval measured for the other batches of 63−125 μm ISG glass grains (see Table 2) and was almost identical for Type S glass beads. Moreover, no change in particle size distribution was observed (Fig. 8a). Such results are consistent with molecular dynamics simulations, which show that at the first moments of contact between water and a glass containing 48.7 mol
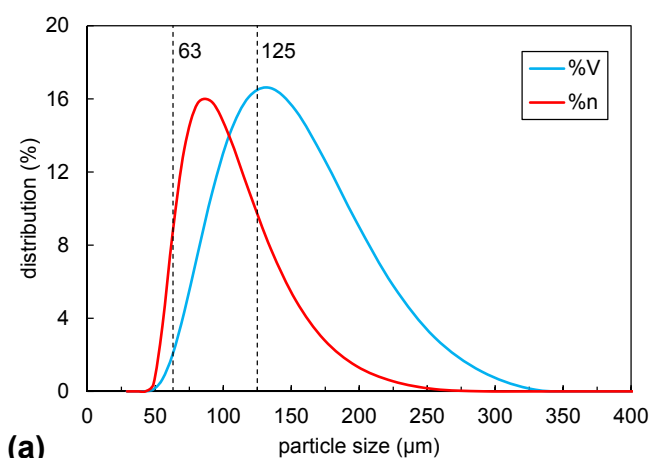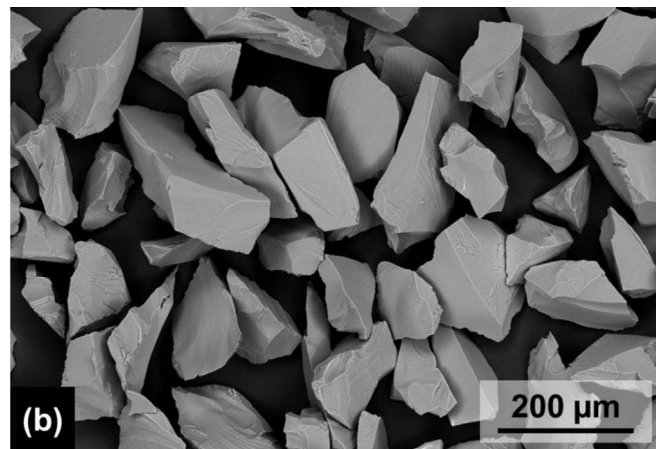
Fig. 2. (a) Particle size distribution for ISG glass grains sieved between 63 and 125 μm (batch B3). The laser diffraction provides a volume distribution assuming spherical particles (%V) from which a size distribution by number of particles is calculated (%n). (b) SEM image of ISG glass grains sieved between 63 and 125 μm (batch B3) and washed with acetone and absolute ethanol to remove fine particles.

% of soluble species, a release of soluble species before any dissolution of the silicate network creates small 2 nm surface irregularities [50]. This value is of the same order of magnitude as the root-mean-square roughness measured by AFM on final-polished monoliths with 0.05 μm diamond suspension [41].
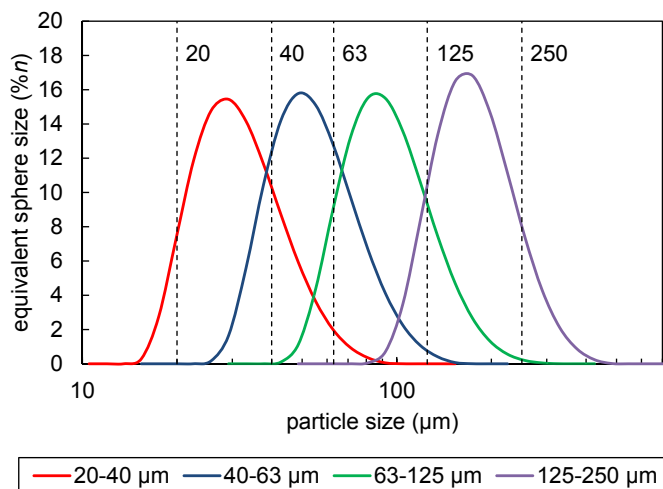
Fig. 3. Particle size distributions for ISG glass grains sieved between 20 and 40 μm, 40 and 63 μm, 63 and 125 μm, 125 and 250 μm.

3.2.2. Annealing

One possible explanation for the differences between the measured rates on powder and monoliths is the effect of powders preparation by crushing. Why this idea? Niu et al. [40] show that a glass surface indentation results in a densification causing a preferential alteration zones. However, during crushing, it is possible that shocks to the glass induce structural modifications causing a preferential alteration of the material.

To test this hypothesis, we postulated that the conclusions drawn for indentations can be extended to defects induced by crushing. It is now well known that the annealing of an oxide glass at a temperature substantially below the glass transition temperature (T_g) allows "curing" of high pressure-induced permanent densification [51,52]. This curing is effective from approximately $0.5 \times T_g$ [53], right from the first moments of annealing [54], because the glass viscosity becomes low enough to allow reorganization within the silicate network. When a densified glass is leached, dissolution is faster at the bottom and on the periphery of the densified zone than on the pristine glass surface [40]. After annealing for 2 h at $0.9 \times T_g$, the glass dissolution front progresses at the same rate on densified and on pristine glasses: the glass is then said to be "cured" [40].

Annealing of glass powder significantly changes the glass specific surface area measured by the BET method (−15%, Table 4) without any modification to particle size distribution (Fig. 8b). This change in S_{BET} therefore cannot be explained by grain agglomeration during annealing, but probably by surface state modifications. If any structural changes due to crushing were cured by annealing, it would then have been expected to see a decrease in the initial rate of annealed powders (ISGa-ST-P63/125), but the opposite was observed. This is likely because annealing significantly reduces the powder reactive surface: the flexibility of the glass network reached during annealing may therefore flatten some roughness. However, this explanation could not be verified because AFM characterization could not be successfully carried out on the glass powders (see section 3.1.3.2).

It is possible to conclude that the observations made on indented glass surfaces are not representative of possible structural modifications of glasses during crushing. This helps to rule out the creation of reactive surface sites by crushing. Moreover, even if some roughness are effectively flattened by annealing, the measured differences on the BET specific surface area do not explain the gap with alteration rates measured on monoliths (see section 3.3).

For annealed monoliths (ISGa-ST-M), the initial dissolution rate remains unchanged. AFM characterizations show that the roughness of the surface area remained unchanged after annealing. No impact of annealing was observed neither on dissolution rate, nor on ISG glass polished monoliths roughness.

3.3. Initial dissolution rate measurements

All leaching tests were carried out at 90 °C and $pH_{90 °C} = 10$. These tests involved two glasses (ISG and Type S) with particles (powder or beads) of various sizes and monoliths. Each measurement was repeated at least twice. The overall results are summarized in Table 5, where initial dissolution rates measured on particles were normalized to their specific and geometric surface (taking into account or not the particle size distribution). The excellent linearity of the tests is demonstrated by the coefficient σ_s/s—representing the ratio between the standard deviation of the slope and the value of the slope—corresponding to correlation coefficients r^2 greater than 0.99.

Glass constituent concentration measurements (e.g. Fig. 9) show that (i) silicon concentration measurements by spectrophotometry and ICP-OES are consistent, (ii) glass dissolution is congruent (i.e. glass constituents dissolve simultaneously, and their stoichiometric ratio in solution is identical to that of the starting material) throughout the experiment and (iii) the release of the glass components is linear (except for Zr, always below the detection limit).

The reproducibility of the measurements was tested by using (i) five 63−125 μm ISG glass powder batches prepared independently (test series ISG-ST-P63/125-By-1, $y = 1$−5), (ii) five tests on the same powder batch (test series ISG-ST-P63/125-B4-x, $x = 1$−5) and (iii) five tests on monoliths (test series ISG-ST-M-z, $z = 1$−5). For these three test series, the good repeatability of rate measurements can easily be seen through silicon concentration measurements plotted versus time in Fig. 10.

There is an evolution of the coefficient of variation between these series of tests (Table 6): it is lower when measurements were performed on the same glass powder batch, but multiplied by a factor of ≈2 when other batches of the same particle size were used and by ≈ 3 when other particle sizes were used. All results obtained on ISG powders are consistent within a maximum uncertainty of ±20%.

Such results are confirmed when using Type S glass beads: rate measurements are repeatable within the same particle size, but the variations are larger from one particle size to another. Results are consistent with a maximum uncertainty of ±25%.

The comparison of r_0 obtained on ISG glass powders normalized to S_{geo} or S_{BET} with r_0 measured on ISG glass monoliths shows that r_0 normalized to S_{geo} are closer to those obtained on monoliths but do not overlap (Fig. 11a). It could be summarized as follows: $r_{0, geo}$ (powder) ≈ $r_{0, geo-psd}$ (powder) > $r_{0, geo}$ (monolith) ≫ $r_{0, BET}$ (powder). For Type S glass (Fig. 11b), a small difference could be noticed between $r_{0, geo-psd}$ and $r_{0, geo}$ because of the bead distributions in the size range (Fig. 4a). The most noticeable observation is that Type S glass $r_{0, geo}$ (monolith) is comparable with $r_{0, geo}$ (beads), indicating that geometric surface is a good way to estimate glass reactive surface when the geometry of objects can be perfectly described. As for ISG powder, the specific surface area measured by gas adsorption on Type S glass beads overestimates the reactive surface.

It was important to check whether there might be a dependence of the initial dissolution rate measured on the experimental
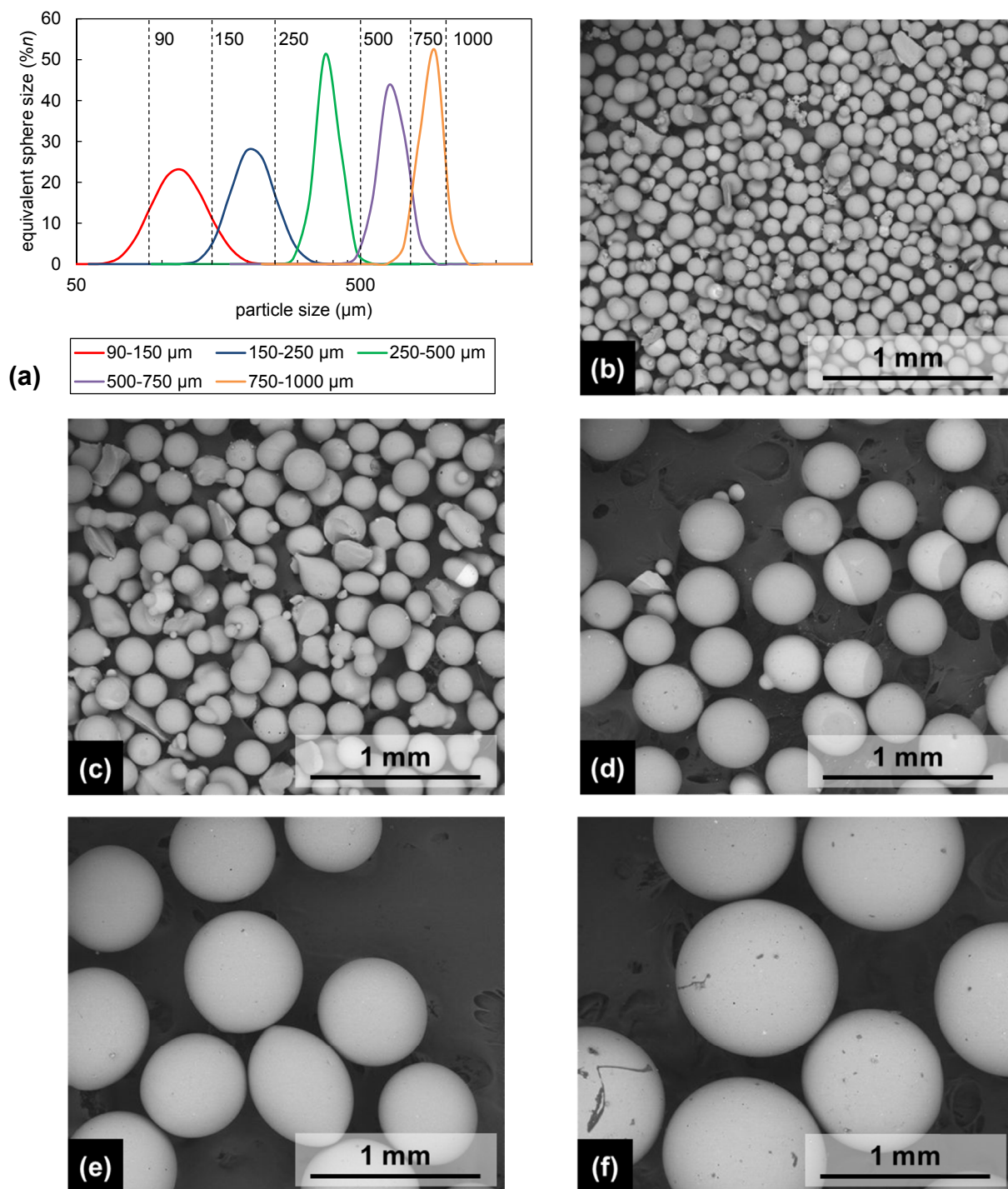
Fig. 4. (a) Particle size distributions and SEM images of Type S SiLibeads® glass beads (b) 90−150 μm, (c) 150−250 μm, (d) 250−500 μm, (e) 500−750 μm and (f) 750−1000 μm. Such particles present high roundness. However, some of them are ovoid or have surface protuberances, and some have indefinite shapes. These defects are more present for smaller particle sizes.

procedure used. For this, SPFT and MCFT tests were carried out to compare with the static tests presented above. These different test types were conducted at the same temperature and pH as the static tests. SPFT conducted on ISG glass powder gave slightly higher results than the associated static tests (Fig. 12a), but the data remain consistent. For the MCFT test method, even if results are more dispersed (Fig. 12b), the conclusion remains the same.

4. Discussion

4.1. Repeatability and precision of initial rate measurements

The evolution of the coefficient of variation for the test series is worth discussing (Table 6). Firstly, the lowest coefficient of variation was found for measurements performed on the same powder
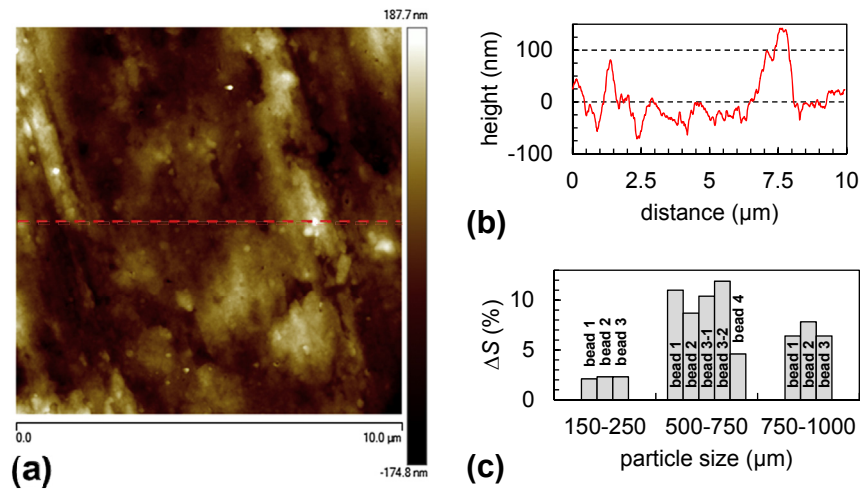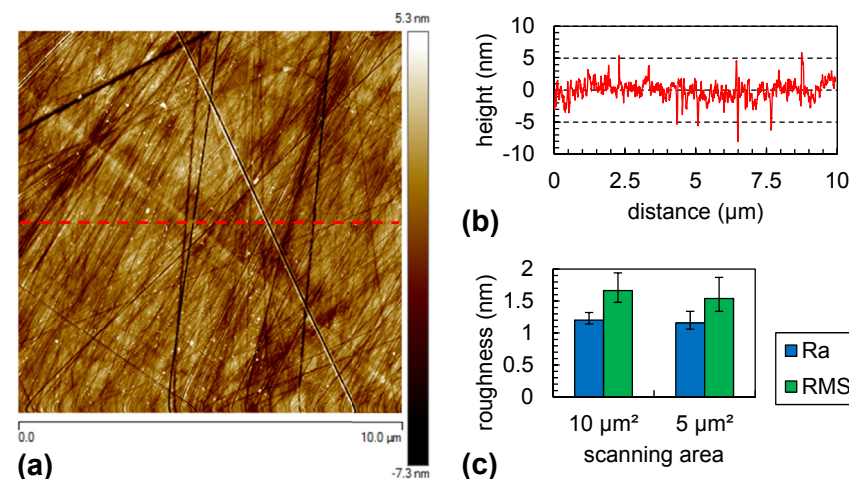
Fig. 5. (a) 10 μm × 10 μm Tapping mode AFM image (b) with height-distance profile along the dotted line of a Type S glass bead (500−750 μm, bead 1). (c) ΔS measurements for three particle sizes.
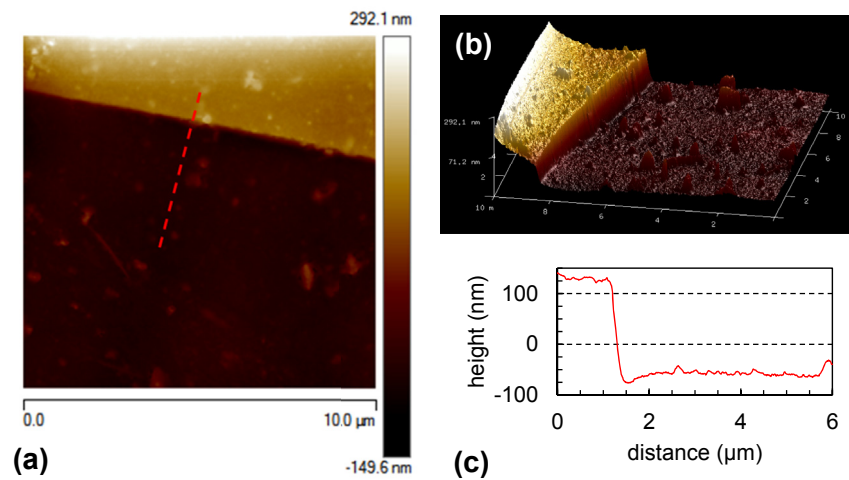
Fig. 6. (a, b) 10 μm × 10 μm Tapping mode AFM images (c) with height-distance profile along the dotted line of an ISG glass crushed particles.

Fig. 7. (a) 10 μm × 10 μm Peak Force mode AFM image (b) with height-distance profile along the dotted line and (c) roughness measurements of the polished ISG monolith.

Table 3
Literature data on the roughness measured on glass monoliths having a surface polished by different methods.

Glass	Surface type	R_a (nm)	R_{ms} (nm)	Reference
Albite glass	Final polish 0.05 μm	–	2.02 ± 0.19	[63]
Calcium aluminum silicate glass (CAS1509)	Final polish 0.1 μm	–	3.46	[64]
ISG	Final polish 1 μm	–	$\approx 1 \cdot 10^1$	[49]
ISG	Final polish 1 μm	1.18	1.60	This work
Model soda lime glass	Fire polish	–	0.3	[60]
R7T7	Final polish 1 μm	$2 \cdot 10^1$	–	[59]
R7T7	Fire polish	$1 \cdot 10^1$	–	[59]

Table 4
Comparisons of specific surface areas (BET model, S_{BET}) before and after two post-treatments: washing with water for 15 min at room temperature and annealing at $0.9 \times T_g$ for 2 h.

Glass	Size fraction (μm)	Post-treatment	S_{BET} before post-treatment (cm^2 g^{-1})	S_{BET} after post-treatment (cm^2 g^{-1})
ISG	63–125 B2	washing with water	645	600
Type S	90–150	washing with water	270	268
ISG	63–125 B5	annealing	600	525
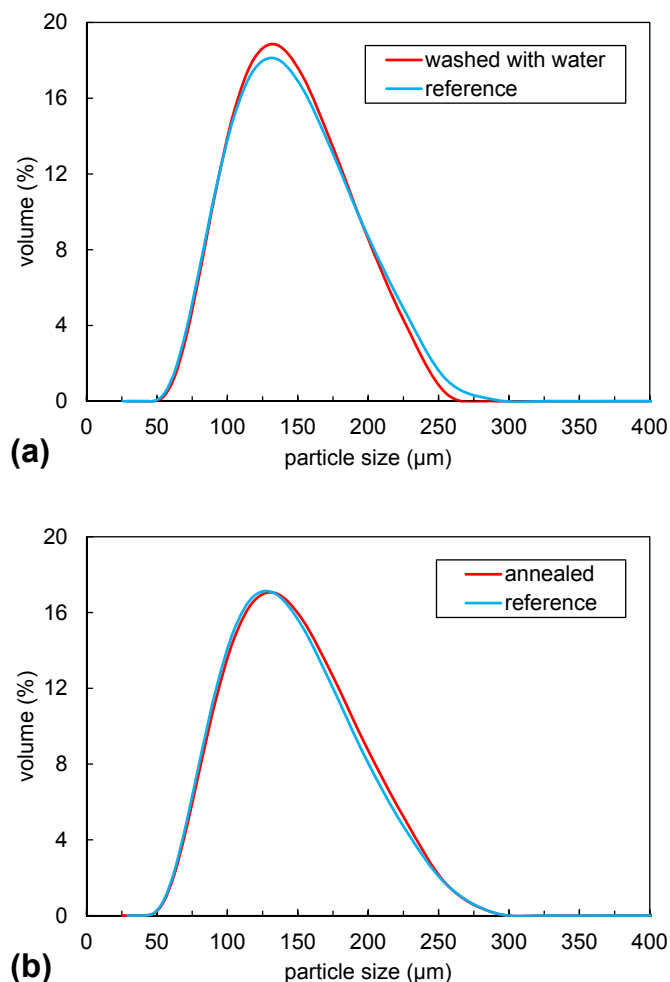
Fig. 8. Comparisons of particle size distributions for ISG glass grains before and after (a) washing with water for 15 min at room temperature and (b) annealing at $0.9 \times T_g$ for 2 h.

the mean surface area of the sample: the preparation protocol seems therefore to ensure good sample homogeneity. The coefficient of variation then increases by a factor of ≈ 3 when different powder batches are tested (ISG-ST-P63/125-By-1 and ISG-ST-P), showing the low impact of sample preparation on the rate measurements.

From these results, it is possible to conclude that: (i) the data set is consistent, (ii) the various tests used are consistent and (iii) measurements are repeatable. Unfortunately, it appears that to be able to provide strong statistical data, more tests are required. Moreover, quantifying static test reproducibility (as defined in ISO 3534–1 [38]) would require the involvement of other laboratories.

The consistency of values from the various types of r_0 measurement tests validates the use of the different protocols employed by international laboratories working on long term behavior of glass. These protocols can therefore be run interchangeably depending on the objectives given for the study beyond simple rate measurement (e.g. MCFT is the only experimental protocol permitting the characterization of the entire leached surface, because of the small size of the area brought into contact with water). Note that soxhlet—one of the devices commonly used for r_0 measurements—was not considered in this study because it only allows glass dissolution in pure water and would therefore not allow the use of the KOH solution.

Considering the static test results, data dispersion is higher for Type S glass than for ISG. This can be explained by a composition effect. The ISG glass used in this study comes from the same preparation carried out by the Mo-Sci Corporation and shipped to international laboratories to facilitate result comparisons. The situation is different for Type S glass, manufactured for industrial purposes: the leached samples may come from different production runs, which can lead to small variations in glass composition within the tolerances defined in Table 1.

The $\pm 10\%$ uncertainty on the determination of initial rates announced elsewhere [11] is valid only if the measurements are performed under specific conditions favoring low dispersion data (e.g. same glass batch, protocol, equipment, operator). It appears that a minimum uncertainty of 25% for r_0 measurements by static test is more realistic. This uncertainty is close to that announced for SPFT [21,27,55]. Moreover, it must be remembered that high values for both temperature and pH were chosen in order to simplify the measurements; one can therefore expect an increase of these uncertainties at lower temperature and near-neutral pH.

batch from the same preparation (ISG-ST-P63/125-B4-x). This result is significant in view of the small amount of powder used in this type of test and whose surface area could vary significantly from

Table 5
Initial rate measurements normalized to S_{geo}, $S_{geo\text{-}psd}$ and S_{BET} for particles and S_{geo} for monoliths. Rates are expressed in g m^{-2} d^{-1}. Test name includes glass name (ISG or S), test performed (ST, SPFT or MCFT), sample shape (P for particles—powders or beads—and M for monolith) and replicate number. σ_s/s represents the ratio between the standard deviation of slope and the value of the slope for the linear regression permitting the rate calculation. The letter "a" after glass name indicates that glass sample was annealed at $0.9 \times T_g$ for 2 h. Graphical representations of these results, more easily readable, are shown in Fig. 11 and Fig. 12.

| Test name	Glass	Sample	Test	σ_s/s ($\times 10^{-2}$)	$r_{0\ geo}$	$r_{0\ geo\text{-}psd}$	r_{BET}
ISG-ST-M-1	ISG	Monolith	ST	4.49	10.59	–	–
ISG-ST-M-2	ISG	Monolith	ST	5.93	11.99	–	–
ISG-ST-M-3	ISG	Monolith	ST	2.86	11.14	–	–
ISG-ST-M-4	ISG	Monolith	ST	5.83	11.33	–	–
ISG-ST-M-5	ISG	Monolith	ST	5.42	10.78	–	–
ISG-MCFT-M-1	ISG	Monolith	MCFT	0.30	13.03	–	–
ISG-MCFT-M-2	ISG	Monolith	MCFT	0.39	9.78	–	–
ISG-MCFT-M-3	ISG	Monolith	MCFT	0.83	9.58	–	–
ISG-ST-P20/40-1	ISG	Powder 20−40 µm	ST	3.22	13.24	14.05	5.13
ISG-ST-P20/40-2	ISG	Powder 20−40 µm	ST	3.58	12.76	13.54	4.94
ISG-ST-P40/63-1	ISG	Powder 40−63 µm	ST	0.97	14.55	15.41	6.05
ISG-ST-P40/63-2	ISG	Powder 40−63 µm	ST	3.57	13.04	13.81	5.43
ISG-ST-P63/125-B1-1	ISG	Powder 63−125 µm	ST	2.66	15.95	16.11	6.41
ISG-ST-P63/125-B2-1	ISG	Powder 63−125 µm	ST	3.16	14.73	15.73	5.83
ISG-ST-P63/125-B3-1	ISG	Powder 63−125 µm	ST	2.98	15.93	16.07	6.21
ISG-ST-P63/125-B4-1	ISG	Powder 63−125 µm	ST	1.96	13.96	14.37	5.66
ISG-ST-P63/125-B4-2	ISG	Powder 63−125 µm	ST	1.97	14.57	15.00	5.90
ISG-ST-P63/125-B4-3	ISG	Powder 63−125 µm	ST	1.25	13.76	14.16	5.57
ISG-ST-P63/125-B4-4	ISG	Powder 63−125 µm	ST	2.01	14.57	15.00	5.90
ISG-ST-P63/125-B4-5	ISG	Powder 63−125 µm	ST	0.82	14.29	14.71	5.79
ISG-ST-P63/125-B5-1	ISG	Powder 63−125 µm	ST	1.88	14.34	14.77	6.10
ISG-ST-P125/250-1	ISG	Powder 125−250 µm	ST	1.86	16.38	15.76	6.08
ISG-ST-P125/250-2	ISG	Powder 125−250 µm	ST	1.31	16.98	16.34	6.30
ISG-SPFT-P63/125-B4-1	ISG	powder 63−125 µm	SPFT	1.24	17.11	16.53	6.93
ISG-SPFT-P63/125-B4-2	ISG	Powder 63−125 µm	SPFT	5.69	16.28	15.72	6.59
ISGa-ST-M-1	ISG	Monolith	ST	4.18	10.88	–	–
ISGa-ST-M-2	ISG	Monolith	ST	4.01	10.63	–	–
ISGa-ST-P63/125-1	ISG	Powder 63−125 µm	ST	0.73	16.02	15.96	7.78
ISGa-ST-P63/125-2	ISG	Powder 63−125 µm	ST	3.61	17.54	17.61	7.92
S-ST-B90/150-1	Type S	Beads 90−150 µm	ST	0.55	5.95	5.95	4.41
S-ST-B90/150-2	Type S	Beads 90−150 µm	ST	1.66	6.11	6.11	4.52
S-ST-B150/250-1	Type S	Beads 150−250 µm	ST	2.03	5.08	5.60	3.94
S-ST-B150/250-2	Type S	Beads 150−250 µm	ST	2.10	5.17	5.69	4.00
S-ST-B250/500-1	Type S	Beads 250−500 µm	ST	2.31	5.48	5.94	2.80
S-ST-B250/500-2	Type S	Beads 250−500 µm	ST	3.63	6.48	7.03	3.32
S-ST-B500/750-1	Type S	beads 500−750 µm	ST	3.64	7.56	8.21	3.83
S-ST-B500/750-2	Type S	Beads 500−750 µm	ST	1.54	6.98	7.65	3.57
S-ST-B750/1000-1	Type S	Beads 750−1000 µm	ST	4.22	6.98	7.25	3.70
S-ST-B750/1000-2	Type S	Beads 750−1000 µm	ST	1.06	7.06	7.63	3.74
S-ST-M-1	Type S	Monolith	ST	2.47	6.23	–	–
S-ST-M-2	Type S	Monolith	ST	2.30	5.56	–	–
S-ST-M-3	Type S	Monolith	ST	2.57	6.41	–	–
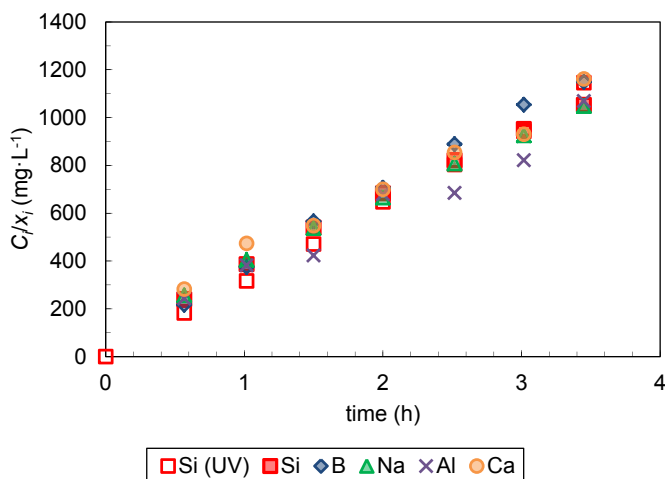
Fig. 9. Example of linear and congruent dissolution of an ISG glass monolith (test ISG-ST-M-3) at 90 °C, pH = 10. Data are expressed as the elemental concentration C_i normalized to the weight glass content x_i in element i. Concentrations were measured by ICP-OES (solid squares) and spectrophotometry (empty squares) for Si; by ICP-OES for other elements. Zr concentrations were always below the detection limit.

4.2. Remarks on surface measurements

4.2.1. Fragmented material

In the ideal case of a material fragmented into identical spheres of radius R, the area of each sphere is $4 \cdot \pi \cdot R^2$ and their number per volume unit is $3/(4 \cdot \pi \cdot R^3)$. The total surface area developed by these spheres is $12 \cdot \pi \cdot R^2/(4 \cdot \pi \cdot R^3) = 3/R$ and their specific surface area $3/\rho \cdot R$ (with ρ the density of the solid). The specific surface area is inversely proportional to the radius of the particle, meaning that knowledge of R is crucial. The case of perfect smooth spheres in no way describes glass grains in reality, because (i) there is a distribution of particle sizes and (ii) there are irregular particle shapes, with conchoidal fractures that appear during glass crushing. The glass particles size distributions can be categorized between Gaussian distribution and positive skewed distribution, which conforms to the log normal distribution. Geometric calculations cannot describe properly the surface of crushed glass particles well.

To get closer to the specific surface area of a non-porous fragmented solid, gas adsorption onto the solid surface can, in principle, provide useful information: the reactive surface is then assumed to be proportional to the BET specific surface area. It is particularly interesting in the case of powders, whose size distributions and
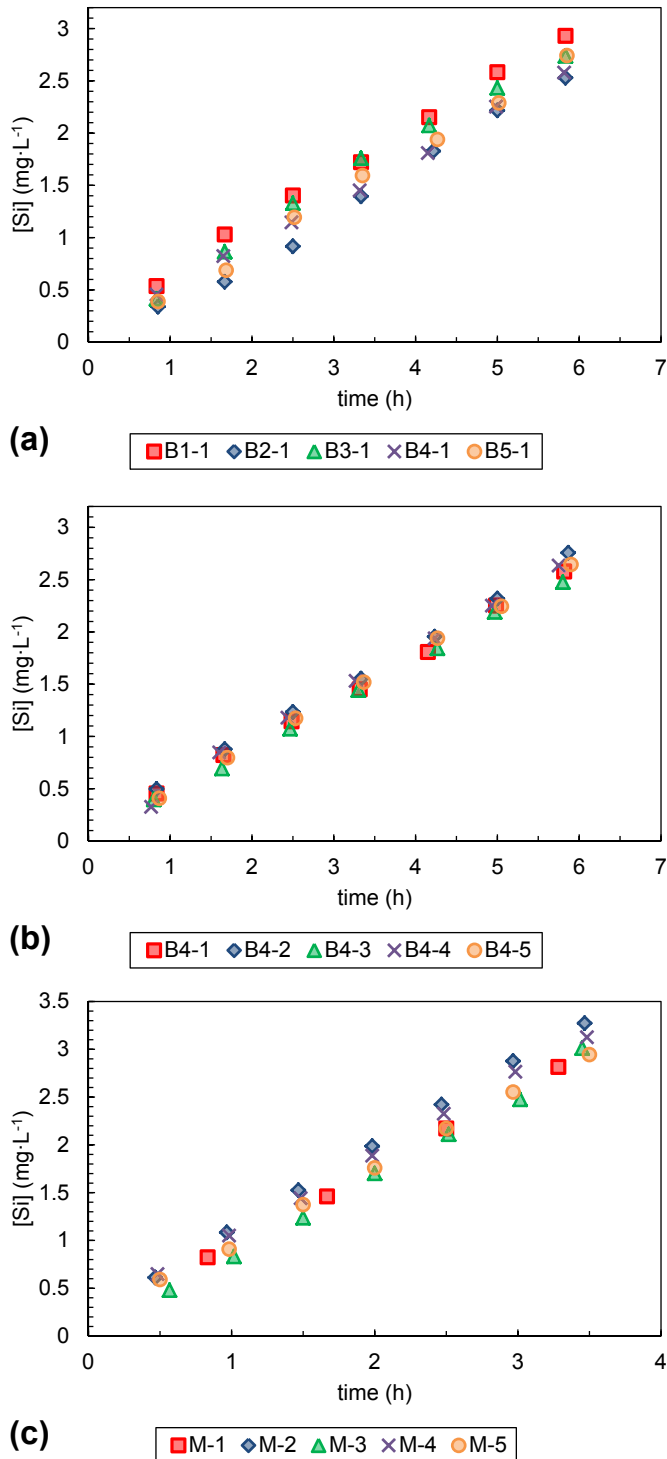
Fig. 10. Silicon concentrations versus time for test series (a) ISG-ST-P63/125-B*y*-1 performed on powder independently prepared batches, (b) ISG-ST-P63/125-B4-*x* performed on the same powder batch and (c) ISG-ST-M-*z* performed on monoliths.

shapes are too complex to be accurately described geometrically or by simple but probably long, tedious and largely unproductive microscopy techniques. Currently, the most popular model used to interpret the so-called Type II isotherms is the BET model [17]. For non-porous or macroporous solids, the Type II isotherm represents unrestricted monolayer-multilayer adsorption [56]. While BET equations are widely recognized, they are criticized because they

assume that all adsorption sites are energetically identical. Moreover, the model focuses on the interactions between the surface and gas molecules but neglects the interactions between the gas molecules themselves. In "very favorable" cases of measurements with nitrogen or argon, an uncertainty of ±10% must be taken into account for the results [48,57] and results may vary significantly depending on the adsorbate gas used [58]. Krypton is routinely used for relatively low surface determination because of its low saturated vapor pressure, but the measurement uncertainty can then rise to about ±20% because data interpretation may be more difficult. However, even with such an error, the initial dissolution rates of glass powders normalized to their specific surface area are far from those measured with monoliths.

4.2.2. Polished monoliths

Taking the geometric surface area of a monolith as a reference for determining the reactive surface area requires ensured measurement accuracy. In particular, monolith roughness has an impact on the dissolution rates measured: the rougher it is, the higher the dissolution rate normalized to S_{geo} is during the first moments of the initial dissolution rate measurement [59]. The effect of roughness decreases with the ingress of the dissolution front because dissolution acts as a "chemical polishing". In the study by Dussossoy et al. [59], the ratio between the initial dissolution rate of an "as cut" monolith (1.6 μm of average roughness R_a) and of a polished monolith (polished with 1 μm diamond suspension, $R_a = 0.02$ μm) is 1.8 after 7 days and is then reduced to 1.3 after 28 days. The polished monolith dissolution rate remains the same over time, while that of the "as cut" one decreases. These results indicate that the chemical polishing is not active on the polished monolith, so that its roughness is negligible compared to the penetration depth of the dissolution front. These results—added to those displayed in section 3.1.3.3 showing that the ΔS of a polished monolith (final polishing 1 μm diamond paste) does not exceed 1%—confirm that the determination of geometric surface of a polished monolith by a simple measurement with a digital caliper is accurate at least up to scale probed by the tip of the AFM.

4.2.3. Potential contributions from roughness

If the rate measured on a polished monolith is taken as a reference, the rate measured on powder and normalized to S_{BET} is underestimated by a factor of ≈2, while the rate normalized to S_{geo} is overestimated by a factor of 1.3. It is undeniable that the r_0 normalized to S_{geo} is closer to that measured on monoliths, despite the fact that the assumption of spherical particles of identical radius does not describe glass powders well.

One hypothesis proposed by the authors to explain the underestimation of the rate normalized to the specific surface area—and thus the overestimation of the reactive surface area measured by the BET method—is the existence of what may be called a (i) *shape factor F_s* (Eq. (10)) expressing the difference between the real shape of the grain and a sphere and (ii) a *roughness factor F_r* (Eq. (11)) due to grain surface irregularities. The S_{BET}/S_{geo} ratio could thus be explained as $F_s \times F_r$. For ISG glass, it is possible to estimate $F_s = 1.3$ and $F_r = 1.9$. Similarly, for Type S glass, F_s is close to 1 and $F_r = 1.6$. Because of the spherical shape of Type S glass beads, it is logical to obtain F_s (Type S) = $1 < F_s$ (ISG).

$$F_s = \frac{S_{geo}(\text{monolith})}{S_{geo}(\text{particles})} \propto \frac{r_{0, geo}(\text{particles})}{r_{0, geo}(\text{monolith})} \qquad (10)$$
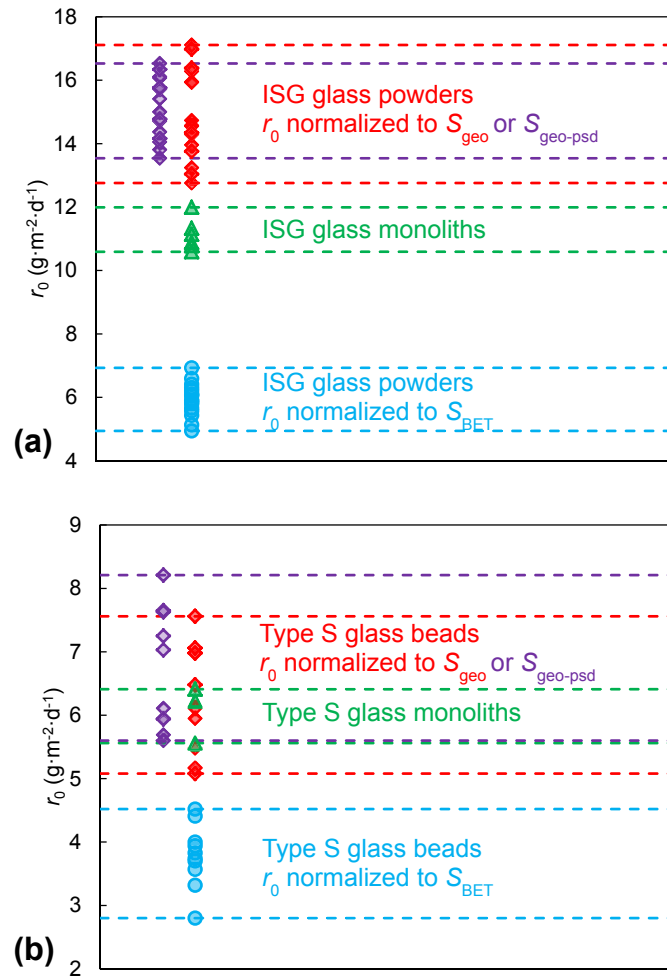
$$F_r = \frac{S_{BET}(\text{particles})}{S_{geo}(\text{monolith})} \propto \frac{r_{0, geo}(\text{monolith})}{r_{0, BET}(\text{particles})} \qquad (11)$$

Table 6
Statistical data for test series conducted at 90 °C, pH = 10 on the same ISG powder batch (ISG-ST-P63/125-B4-x, x = 1 to 5), on five ISG 63−125 μm powder batches prepared independently (ISG-ST-P63-125By-1, y = 1 to 5), on all static tests performed on ISG glass powders (ISG-ST-P), monoliths (ISG-ST-M) and Type S glass beads (S-ST-P). $<r_0>$ (g m^{-2} d^{-1}) represents the average initial dissolution rate calculated on the number of tests indicated in the second column and the coefficient of variation c_v is the ratio of the standard deviation to the mean.
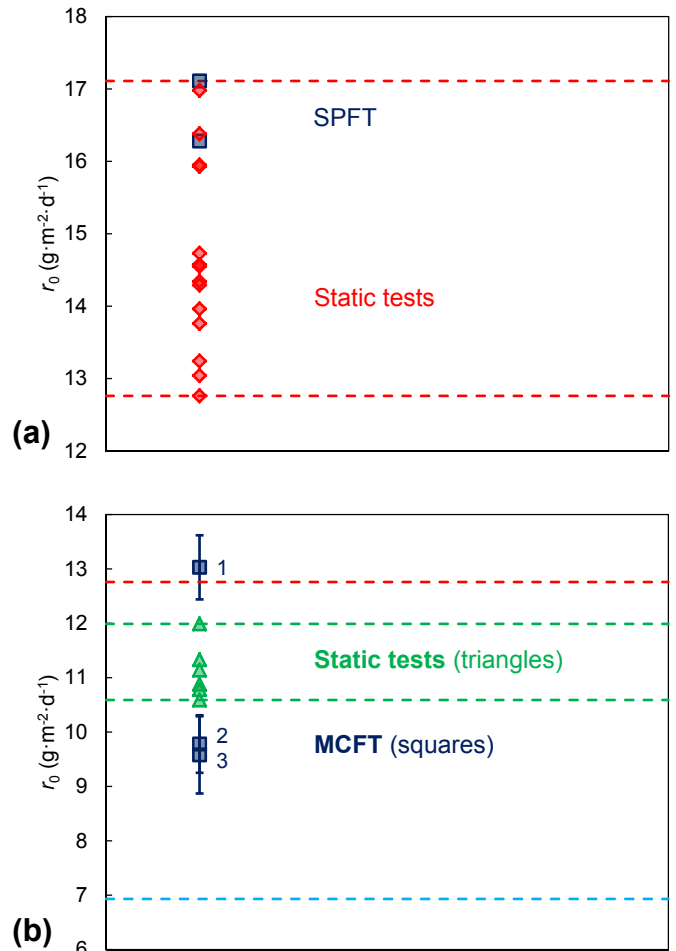
Test series	Number of tests	$<r_0>_{geo}$	$c_{v\ geo}$ ($\times 10^{-2}$)	$<r_0>_{geo-psd}$	$c_{v\ geo-psd}$ ($\times 10^{-2}$)	$<r_0>_{BET}$	$c_{v\ BET}$ ($\times 10^{-2}$)
ISG-ST-P63/125-B4-x	5	14.23	2.55	14.65	2.57	5.76	2.55
ISG-ST-P63-125By-1	5	14.98	6.11	15.41	5.15	6.04	4.95
ISG-ST-P	15	14.60	8.46	14.99	5.95	5.82	7.16
ISG-ST-M	5	11.12	4.51	–	–	–	–
S-ST-P	10	6.29	13.7	6.71	14.2	3.78	13.2
S-ST-M	3	6.07	7.38	–	–	–	–

Fig. 11. Comparison between initial dissolution rate measurements performed on (a) ISG glass and (b) Type S glass. Measurements were performed on glass monoliths (triangles) and glass particles of various size fractions normalized to geometric (diamonds) or specific (circles) surface areas. To be easily compared, r_0 values are represented on a single column (except for measurements normalized to $S_{geo-psd}$, shifted for readability).

Fig. 12. (a) Results of SPFT tests on ISG glass powder compared with those of static tests. (b) Results of MCFT tests on ISG monoliths compared with those of static tests: monolith 1 was prepared by the CEA and leached by Kyushu University, monolith 2 was re-polished from monolith 1 and leached by Kyushu University, and monolith 3 was prepared and leached by Kyushu University. Dotted lines are the same as represented in Figure 11.a. To be easily compared, r_0 values are represented on a single column.

AFM measurements conducted on glass beads show that the greater the roughness is, the greater is the gap between $r_{0,\ geo}$ (beads) and $r_{0,\ geo}$ (monolith). Nevertheless, the surface increase ΔS (up to 10%) cannot completely explain a F_r of 1.6. These findings can be extrapolated to crushed glass particles, although AFM measurements were unrepresentative.

Therefore, there is a difference between surface areas measured by AFM or gas adsorption. In the case of nonporous particles, such as those studied here, both techniques measure an external surface.

However, the resolution of the AFM tip (2−20 nm) is large compared with the cross sectional area of Kr atoms (20 Å^2): the surface features measured by those two types of "probes" are different. Then, it appears that the features responsible for the differences between AFM and BET surfaces are "very small", below the sensitivity of AFM. Thus, a surface appearing as relatively flat by microscopy may have a greater BET specific surface area, and vice versa. Such observation was also made on primary silicate minerals by Brantley et al. [66], also indicating that the nature of these small

features and how they interact with water molecules during dissolution experiments are unknown.

4.2.4. What about surface features predominantly contributing to the BET surface area?

Although accessible to gas molecules during specific surface area measurement, the small features—contributing to the F_r factor—are not involved in rate measurement because the irregularity depth is very small compared to the ingress of water. From this point of view, at the very beginning of hydrolysis, a glass grain undergoes what could be called a "chemical polishing" [37,59] by water which flattens the surface, whose chemical composition could then differ significantly from that of the bulk glass [41]. As an example, consider a roughness of 5 nm on ISG glass surface: it will be dissolved in less than 2 min (corresponding to a silicon release of around 20 μg L^{-1}) in the experimental conditions of our study; that explains why such phenomenon could not be seen from solution analysis data. Note that recent studies [37,61] have considered the case of monoliths which all sides are not polished—frequent situation for "small" sides for practical reasons—to see how fast surface roughness are smoothed by aqueous alteration. Under these conditions, the reactive surface is greater than the geometric surface: reactive surface is then determined by dividing the r_0 value measured on a partially polished monolith by that measured on an entirely polished monolith.

5. Conclusions

The results of this study have made it clear that the external surface area measurement of nonporous fragmented materials, with irregular shapes and complex roughness, is particularly difficult. It is challenging to estimate the geometric surface area of such complex objects as crushed glass grains without the use of simplifying assumptions that are difficult to justify. However, the measurement of geometric surface model objects with smooth surfaces, such as beads or parallelepipeds, remains to date the most simple and reliable way to indirectly measure a reactive surface. From a practical point of view, this study has shown that in order to be compared to the dissolution rate measured on polished monoliths, the rate measured on powder ($S_{BET}/S_{geo} \approx 2.5$) and normalized to geometric surface area should be divided by 1.3 while the rate normalized to BET specific surface area should be multiplied by 1.9. The uncertainty of such rate measurements in initial rate regime can reach $\pm 25\%$. A factor of 2 on rate measurements associated with an estimated uncertainty of $\pm 25\%$ largely explain why the debate around glass reactive surface has continued for so long in the community, especially since dissolution rates are rarely measured in such favorable temperature and pH conditions.

The complex shape of the particles and their surface state contribute to the difference between BET specific and geometric surface areas. Difference between these two surface areas has been particularly explained by the presence of small features at the surface of glass particles (typically smaller than the sensitivity of AFM) that mainly contribute to the BET specific surface area. Their nature and the way they interact with water are unknown. Results obtained here suggest that surface developed by such features should not be taken into account in the rate calculations, because the thickness of the altered glass quickly becomes much greater than the roughness heights. Under these conditions, surface area measurement by gas adsorption is not adapted to the determination of reactive surface.

Tests conducted in this study show good repeatability of static tests—very simple to implement for initial rate measurements—regardless of the sample type. The use of other types of tests also gave consistent results.

References

[1] J.D. Vienna, J.V. Ryan, S. Gin, Y. Inagaki, Int. J. Appl. Glass Sci. 4 (2013) 283–294.
[2] S. Gin, A. Abdelouas, L.J. Criscenti, W.L. Ebert, K. Ferrand, T. Geisler, M.T. Harrison, Y. Inagaki, S. Mitsui, K.T. Mueller, J.C. Marra, C.G. Pantano, E.M. Pierce, J.V. Ryan, J.M. Schofield, C.I. Steefel, J.D. Vienna, Mater. Today 16 (2013) 243–248.
[3] D.M. Strachan, J. Nucl. Mater. 298 (2001) 69–77.
[4] C. Poinssot, S. Gin, J. Nucl. Mater. 420 (2012) 182–192.
[5] ASTM International, Standard Practice for Prediction of the Long-term Behavior of Materials, Including Waste Forms, Used in Engineered Barrier Systems (EBS) for Geological Disposal of High-level Radioactive Waste, ASTM Standard C1174, 2007.
[6] P. Van Iseghem, M. Aertsens, S. Gin, D. Deneele, B. Grambow, D. Strachan, P. McGrail, G. Wicks, Ceram. Trans. 207 (2009) 115–126.
[7] J. Neeway, A. Abdelouas, B. Grambow, S. Schumacher, J. Nucl. Mater. 415 (2011) 31–37.
[8] E. Curti, D. Grolimund, C.N. Borca, Appl. Geochem. 27 (2012) 56–63.
[9] E. Curti, J.L. Crovisier, G. Morvan, A.M. Karpoff, Appl. Geochem. 21 (2006) 1152–1168.
[10] A. Abdelouas, K. Ferrand, B. Grambow, T. Mennecart, M. Fattahi, G. Blondiaux, C. Houee-Levin, Mater. Res. Soc. Symp. Proc. 807 (2004) 175–180.
[11] S. Gin, X. Beaudoux, F. Angéli, C. Jégou, N. Godon, J. Non Cryst. Solids 358 (2012) 2559–2570.
[12] W.L. Ebert, M.A. Lewis, N.L. Dietz, Ceram. Trans. 132 (2006) 279–285.
[13] C.A. Utton, R.J. Hand, N.C. Hyatt, S.W. Swanton, S.J. Williams, J. Nucl. Mater. 442 (2013) 33–45.
[14] B. Parruzot, P. Jollivet, D. Rébiscoul, S. Gin, Geochim. Cosmochim. Acta 154 (2015) 28–48.
[15] A. Verney-Carron, S. Gin, P. Frugier, G. Libourel, Geochim. Cosmochim. Acta 74 (2010) 2291–2315.
[16] P. Frugier, C. Martin, I. Ribet, T. Advocat, S. Gin, J. Nucl. Mater. 346 (2005) 194–207.
[17] S. Brunauer, P.H. Emmett, E. Teller, J. Am. Chem. Soc. 60 (1938) 309–319.
[18] J. Patyn, P. Van Iseghem, W. Timmermans, Mater. Res. Soc. Symp. Proc. 176 (1989) 299–306.
[19] B.P. McGrail, W.L. Ebert, A.J. Bakel, D.K. Peeler, J. Nucl. Mater. 249 (1997) 175–189.
[20] J.W. Tester, W.G. Worley, B.A. Robinson, C.O. Grigsby, J.L. Feerer, Geochim. Cosmochim. Acta 58 (1994) 2407–2420.
[21] E.M. Pierce, E.A. Rodriguez, L.J. Calligan, W.J. Shaw, B.P. McGrail, Appl. Geochem. 23 (2008) 2559–2573.
[22] E.M. Pierce, B.P. McGrail, P.F. Martin, J. Marra, B.W. Arey, K.N. Geiszler, Appl. Geochem. 22 (2007) 1841–1859.
[23] S.R. Gislason, E.H. Oelkers, Geochim. Cosmochim. Acta 67 (2003) 3817–3832.
[24] C.M. Riley, W.I. Rose, G.J.S. Bluth, J. Geophys. Res. Solid Earth 108 (2003).
[25] O. Ersoy, E. Sen, E. Aydar, I. Tatar, H.H. Celik, J. Volcanol. Geotherm. Res. 196 (2010) 281–286.
[26] C. Papelis, W. Um, C.E. Russell, J.B. Chapman, Colloids Surf. A 215 (2003) 221–239.
[27] E.M. Pierce, L.R. Reed, W.J. Shaw, B.P. McGrail, J.P. Icenhower, C.F. Windisch, E.A. Cordova, J. Broady, Geochim. Cosmochim. Acta 74 (2010) 2634–2654.
[28] I.W. Donald, Waste Immobilization in Glass and Ceramic Based Hosts: Radioactive, Toxic and Hazardous Wastes, John Wiley & Sons Inc, 2010.
[29] C.M. Jantzen, K.G. Brown, J.B. Pickett, Int. J. Appl. Glass Sci. 1 (2010) 38–62.
[30] J.P. Icenhower, C.I. Steefel, J. Nucl. Mater. 439 (2013) 137–147.
[31] Y. Inagaki, T. Kikunaga, K. Idemitsu, T. Arima, Int. J. Appl. Glass Sci. 4 (2013) 317–327.
[32] M. Fournier, P. Frugier, S. Gin, Procedia Mater. Sci. 7 (2014) 202–208.
[33] D. Wolff-Boenisch, S.R. Gislason, E.H. Oelkers, C.V. Putnis, Geochim. Cosmochim. Acta 68 (2004) 4843–4858.
[34] C. Fischer, I. Kurganskaya, T. Schäfer, A. Lüttge, Appl. Geochem. 43 (2014) 132–157.
[35] J.-M. Gautier, E.H. Oelkers, J. Schott, Geochim. Cosmochim. Acta 65 (2001) 1059–1070.
[36] A.A. Jeschke, W. Dreybrodt, Geochim. Cosmochim. Acta 66 (2002) 3055–3062.
[37] S. Gin, P. Jollivet, M. Fournier, C. Berthon, Z. Wang, A. Mitroshkov, Z. Zhu,

J.V. Ryan, Geochim. Cosmochim. Acta 151 (2015) 68—85.

[38] ISO, Statistics - Vocabulary and Symbols - Part 1: General Statistical Terms and Terms Used in Probability, ISO 3534—1, 2006.

[39] ISO, Accuracy (Trueness and Precision) of Measurement Methods and Results - Part 1: General Principles and Definitions, ISO 5725—1, 1994.

[40] Y.-F. Niu, K. Han, J.-P. Guin, Langmuir 28 (2012) 10733—10740.

[41] Y. Gong, A.W. Wren, N.P. Mellott, Appl. Surf. Sci. 324 (2015) 594—604.

[42] Sigmund Lindner, SiLibeads Glass Beads Type S, Microglass Beads, Product Data Sheet, V11/2012, 2013.

[43] H. Makigaki, Y. Inagaki, K. Idemitsu, T. Arima, S. Mitsui, T. Banba, K. Noshita, Mater. Res. Soc. Symp. Proc. 1193 (2009) 307—314.

[44] Y. Inagaki, H. Makigaki, K. Idemitsu, T. Arima, S.-I. Mitsui, K. Noshita, J. Nucl. Sci. Technol. 49 (2012) 438—449.

[45] K. Okuyama, A. Sasahira, K. Noshita, T. Yoshida, K. Kato, S. Nagasaki, T. Ohe, Phys. Chem. Earth 32 (2007) 463—468.

[46] K. Okuyama, A. Sasahira, K. Noshita, T. Ohe, Appl. Geochem. 23 (2008) 2130—2136.

[47] ASTM International, Standard Test Method for Silica in Water, ASTM Standard S859, 2010.

[48] S.J. Gregg, K.S.W. Sing, Adsorption, Surface Area, and Porosity, Academic Press, 1991.

[49] J. Hopf, E.M. Pierce, Procedia Mater. Sci. 7 (2014) 216—222.

[50] J.M. Delaye, A. Kerrache, S. Gin, Chem. Phys. Lett. 588 (2013) 180—183.

[51] J.E. Neely, J.D. Mackenzie, J. Mater. Sci. 3 (1968) 603—609.

[52] Y. Kato, H. Yamazaki, S. Itakura, S. Yoshida, J. Matsuoka, J. Ceram. Soc. Jpn. 119 (2011) 110—115.

[53] S. Yoshida, S. Isono, J. Matsuoka, N. Soga, J. Am. Ceram. Soc. 84 (2001) 2141—2143.

[54] J.D. Mackenzie, J. Am. Ceram. Soc. 46 (1963) 470—476.

[55] J.P. Icenhower, B.P. McGrail, W.J. Shaw, E.M. Pierce, P. Nachimuthu, D.K. Shuh, E.A. Rodriguez, J.L. Steele, Geochim. Cosmochim. Acta 72 (2008) 2767—2788.

[56] K.S.W. Sing, Pure Appl. Chem. 54 (1982) 2201—2218.

[57] D.H. Everett, G.D. Parfitt, K.S.W. Sing, R. Wilson, J. Appl. Chem. Biotech. 24 (1974) 199—219.

[58] S.L. Brantley, N.P. Mellott, Am. Mineral. 85 (2000) 1767—1783.

[59] J.L. Dussossoy, C. Dubois, E. Vernaz, A. Chambaudet, Mater. Res. Soc. Symp. Proc. 257 (1991) 109—115.

[60] E. Rädlein, G.H. Frischat, J. Non Cryst. Solids 222 (1997) 69—82.

[61] S. Gin, P. Jollivet, M. Fournier, F. Angeli, P. Frugier, T. Charpentier, Nat. Commun. 6 (2015) 6360.

[62] J. Marra, C. Crawford, D. Peeler, Letter Report on Compositional Measurements of "Common Simple" Glass, SRNL-L3100-2012-00092, Savannah River National Laboratory, 2012.

[63] N.P. Mellott, S.L. Brantley, C.G. Pantano, Topography of polished plates of albite crystal and glass during dissolution, in: R. Hellmann, S.A. Wood (Eds.), Water-rock Interaction, Ore Deposits, and Environmental Geochemisty: a Tribute to David A. Crerar, The Geochemical Society, 2002, pp. 83—95.

[64] N.P. Mellott, S.L. Brantley, J.P. Hamilton, C.G. Pantano, Surf. Interface Anal. 31 (2001) 362—368.

[65] S. Zellnitz, J.D. Redlinger-Pohn, M. Kappl, H. Schroettner, N.A. Urbanetz, Int. J. Pharm 447 (2013) 132—138.

[66] S.L. Brantley, A.F. White, M.E. Hodson, Surface area of primary silicate minerals, in: B. Jamtveit, P. Meakin (Eds.), Growth, Dissolution and Pattern Formation in Geosystems, Springer, 1999, pp. 291—326.